Catalytic Activity and Stability of Two-Dimensional Materials for the Hydrogen Evolution Reaction

Naiwrit Karmodak and Oliviero Andreussi*

Department of Physics, University of North Texas, Denton, TX 76203, USA

E-mail: oliviero.andreussi@unt.edu

Abstract

The catalytic performances of the surfaces of two-dimensional (2D) materials are investigated by means of accurate computational thermodynamics approaches, based on first-principles simulations. Reliable multiscale continuum embedding models are used to capture the effects of electrochemical environments on the catalytic activity and stability of the materials. The proposed simulation workflow allowed us to screen a large database of candidate 2D compounds, composed of 258 materials that have been recently characterized by simulations as easily exfoliable. Out of the starting database, 15 promising electrocatalysts for the hydrogen evolution reaction (HER) are identified. Among these compounds, CoO_2 and FeS show the lowest overpotentials and considerable aqueous stability at acidic pH.

TOC Graphic

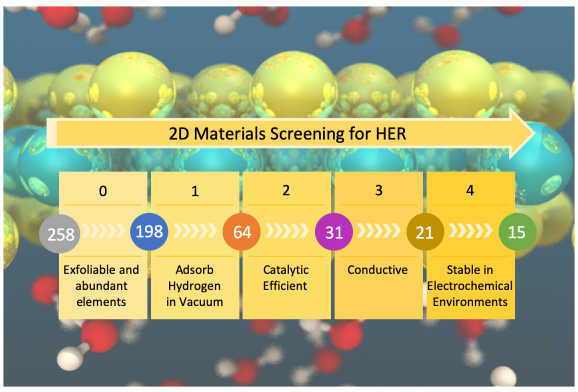

The electrocatalytic reduction of dissolved H^+ ions into molecular hydrogen (H_2) is a key process of any renewable energy technology based on hydrogen fuels.[1] Among several factors, the efficiency of the electrocatalyst is of prime importance in reducing the overall reaction overpotential and enhancing the reaction yield. Pt-group metals have historically been the best performing catalysts. Nevertheless, utilization of these expensive surfaces as electrodes for large scale H_2 generation is a formidable task.[2] Therefore, the search for alternative earth abundant electrocatalysts has attracted huge research interest in the last few years.[3] Here we report a detailed computational screening of the electrocatalytic efficiency of two-dimensional (2D) materials towards the hydrogen evolution reaction (HER) exploiting a first-principles based multiscale approach to electrochemical interfaces. Starting from a computationally generated database of 258 candidate 2D compounds,[4] 15 are identified as promising electrocatalysts for HER, with CoO_2 and FeS showing the best performances and the highest stability to electrochemical conditions.

Indeed, influenced by the extraordinary chemical and physical properties of graphene and layered transition metal-dichalcogenides,[5,6] extensive efforts have been spent in recent years to explore alternative 2D materials and to identify their catalytic properties.[7,8] In particular, when compared to bulk solids, 2D materials intrinsically possess a larger exposed surface, which can substantially enhance their catalytic activity. Large databases of candidate 2D materials have been reported[4,9–13] where structures are proposed by exfoliation of layered 3D solids or by combinatorial substitution of known 2D crystal structures. While most of these

materials have been studied in greater details to understand their electronic structures and physical properties,[4,12,14–16] their applications in electrocatalysis remains less characterized.[17] This is in part due to the challenges involved in the modeling of electrochemical setups, whose multiscale nature makes fully atomistic first-principles simulations impractical for systematic studies.[18,19] However, with the recent advances in continuum solvation models, the accuracy of first-principles based electrochemical simulations has greatly improved. In particular, the recently proposed continuum models of liquid solvents[20] and of the electrochemical diffuse layer[21,22] allow to exploit a rigorous grand potential thermodynamic approach[23] to characterize the stability of electrochemical interfaces. The computationally inexpensive nature of the adopted approach allowed us to perform a systematic analysis of the electrocatalytic efficiency on a large number of candidate materials.

Figure 1 summarizes the simulation workflow of the screening process for the evaluation of the HER performances of 2D materials. The initial database of materials considered in this study is composed of 258 compounds, whose exfoliation (a.k.a. binding) energies computed with density functional theory (DFT) in vacuum, E_b^{vac}, are smaller than 35 meV/Å^2.[24] The, simulations of the electrochemical interfaces are performed with varying number of adsorbed hydrogen species Environment effects, which can play a crucial role in the catalytic efficiency and electrochemical stability of the materials, are included in a progressive way along the screening process. The details of the continuum simulation methods are discussed in the supporting information (SI). Simulations are performed for the isolated 2D materials in vacuum, as well as in a continuum dielectric medium, as modeled by the Self-Consistent Continuum Solvation (SCCS) model.[20] The presence of an electrochemical diffuse layer, described by a continuum charge distribution based on the Gouy-Chapman-Stern model,[25,26] is accounted for in the calculation of the potential-dependent interfacial free energies. From these results, the exfoliation energies for the 2D materials in aqueous medium and electrochemical stability towards decomposition to various aqueous species are determined, showing good agreement with experiments. The adopted approach allowed us to

characterize the overpotentials for H^+ electrosorption as a function of the applied potentials and pH of the medium. Furthermore, the electrical conductivity of the materials is assessed by the calculation of electronic bandgaps, using the DFT+U method, where the Hubbard U parameter is estimated self-consistently through the ACBN0 functional.[27–29] We note here that, in order to distinguish between the hexagonal and trigonal prismatic polymorphs of the transition metal dichalcogenides (MX_2) in the following discussion, these compounds will be labelled as 2H- or 1T-MX_2 respectively, where M corresponds to the transition metal and X to the chalcogenides group.

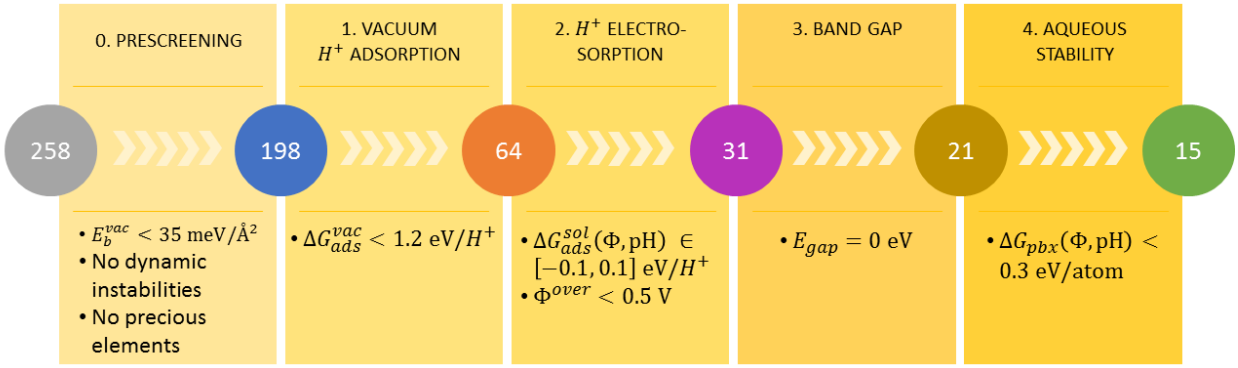

Figure 1: The screening process employed to study the electrocatalytic efficiency of the materials is schematized. The screening criteria are summarized in the bottom section of each step and described in the text. The number of materials considered before and after each screening step is reported within the circular insets.

As a pre-screening step (Figure 1), the monolayers with high negative phonon frequencies are removed from the initial set of materials. Similarly, compounds containing platinum, lanthanide, and actinide group elements are removed, as their scarce natural abundance or stability would hinder large-scale applications. This resulted in 198 potential compounds consisting of 6 unary, 120 binary, and 72 trinary compounds. The adsorption free energies (ΔG_{ads}) of the H^+ ions on the electrode surface represents an important criteria in deciding the overall reaction thermodynamics of the HER process ($2H^+ + 2e \rightleftharpoons H_2$). The electrocatalysts with an optimum value for ΔG_{ads} near to zero show maximum efficiency.[30] Therefore, the first screening of 2D materials is performed depending upon the binding energy of H^+ ions at different surface positions (ontop, bridge, and hollow sites), ΔG_{ads}^{vac}, without the inclusion

of continuum embedding. The 2D materials are fully relaxed in presence of the adsorbed H^+ ions to determine the stability of the compounds. Among the 198 monolayers, 88 compounds show intralayer bond distance elongation by more than 20% after H^+ adsorption. All these materials are found to partially decompose into HX entities, creating vacancies onto the surface layers, where X corresponds to the surface atoms at the adsorption sites. This unstable set of compounds mainly comprises halides, oxyhalides and compounds with larger electronegativity differences between the constituent atoms.

On the resulting set of 110 compounds, the proton adsorption energies (ΔG_{ads}^{vac}) for different H^+ surface coverages varying from 25% to around full coverage are calculated and compared to their exfoliation energies (E_b^{vac}) in Figure 2. The ΔG_{ads}^{vac} of the H^+ ions are found to decrease with the increase in the E_b^{vac}, consistently with an enhancement of the surface reactivity. Based upon the average binding energy values per H atom and the stability with respect to different surface coverage, the materials are classified into two different groups. 42 materials (red circles in Figure 2) are obtained with ΔG_{ads}^{vac} on the basal surfaces greater than 1.2 eV/H atom. In order for these monolayers to bind the H^+ ions, they would need prior activation by introduction of defects, atomic doping, or lateral aligning such that the edge sites become exposed for the reaction. As an example, the transition metal dichalcogenides such as 2H-MoS_2 and 2H-WS_2 belong to this group, for which the edge sites show greater electrocatalytic activity compared to the basal surfaces.[31,32] The other group consisting of the 68 monolayers (blue circles in Figure 2) show H^+ binding energies less than 1.2 eV/Hatom. From this group, we removed the four monolayers with chemical formula NbF_4, Hf_3Te_2, HfSiTe, and ZrSiTe. These compounds are found to prefer interpenetration of H^+ ions between the atomic layers and therefore might not allow for reaction with another H^+ ion to form molecular H_2. The remaining compounds (64, following Step 1 in Figure 1) are identified as suitable candidates and therefore studied for H^+-electrosorption properties with continuum solvation embedding.

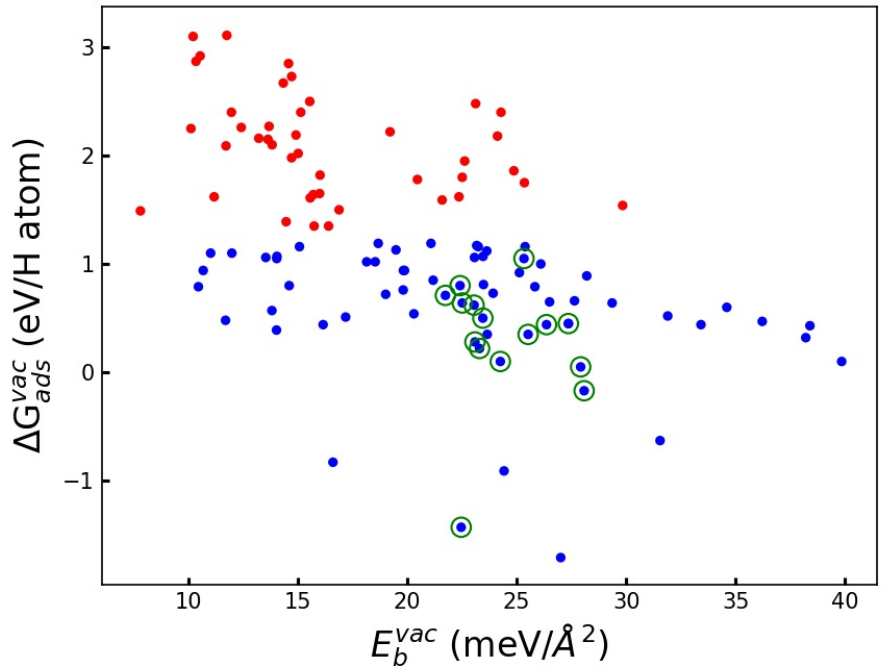

Figure 2: The ΔG_{ads}^{vac} vs E_b^{vac} plot for the 110 2D compounds that are found to be stable after adsorption of H^+ ions at different surface positions. The red/blue circles denote compounds for which ΔG_{ads}^{vac} is greater/lower than 1.2 eV/H atom. The 15 compounds identified by the complete screening procedure as most promising electrocatalysts for HER are denoted by green overcircles.

The H^+ adsorption free energies ($G^{sol}_{ads}(\Phi, pH)$) on the basal surfaces are determined using eq. 1.

$$\Delta G^{sol}_{ads}(\Phi, pH) = J(\Phi, pH) - J(\Phi) + \Delta E_{ZPE} - T\Delta S_{ads} \quad (1)$$

In this equation, $J(\Phi, pH)$ and $J(\Phi)$ denote grand-potential free energies of the 2D material surfaces with and without H^+ adsorption , whereas ΔE_{ZPE} and $T\Delta S_{ads}$ are the zero point energy and entropy correction for the adsorption respectively. The detailed expressions are discussed in section S-II of SI. In order to identify the efficient electrocatalysts among the selected 64 monolayers, the threshold for $G^{sol}_{ads}(\Phi, pH)$) is set between -0.1 to 0.1 eV/H. While the adsorption free energy near to zero is optimal due to better efficiency, compounds with small positive or negative theoretical adsorption free energy values could be used as efficient electrocatalysts for HER.[33] Using these criteria, and focusing the analysis at an acidic pH equal to 1, we obtained 27 2D-materials, which show the H^+ electrosorption overpotentials below 0.5 V vs RHE. Among the remaining compounds, 11 monolayers (1T-MoS_2, FeO_2, NiO_2, GeS, GeSe, SnTe, PbTe, W_3N_2, P(P), As (P), and P(As)) show higher negative binding energies for H^+ ions. For these compounds the pH range is varied up to a value of 7, in order to verify the existence of a pH range for which $G^{sol}_{ads}(\Phi, pH)$ could be tuned to vary between -0.1 to 0.1 eV/H atom. As a result of this process, 4 additional materials (1T-MoS_2, GeS, GeSe, and P(As)) are identified as possible candidates for HER catalysis. Eventually, 17 materials with low adsorption free energy in vacuum are found to require significantly high overpotentials when simulated in a continuum solvation environment. About one fourth of the materials that were identified as promising catalysts based off simulations in vacuum are shown to be ineffective when proper account of the electrochemical environment is included. In particular, for the transition metal-dichalcogenides the trend in catalytic efficiency obtained in electrochemical environments is in better agreement with experimental results.[34] Eventually, for the 9 trinary compounds (TiNBr, TiNCl, TiNI with FeOCl prototype; ZrNBr and ZrNCl with SmSI prototype; Bi_2Te_2S, KTlO with Cu_5FeS_4

prototype; and Bi_2Te_2S, Bi_2Te_2Se with Bi_2Te_2S prototype), the relaxation of the atomic positions in oxidising potentials and continuum electrochemical environments failed to provide stable arrangements.

Therefore, overall 31 2D materials with overpotential values less than 0.5 V (step 2, Figure 1) are obtained, as shown in Table 1. Column 3 gives the corresponding overpotential values with respect to RHE. If pH values greater than 1 are required, the preferred values are indicated within the parentheses.

Besides the ability to reversibly bind hydrogen atoms, the HER catalytic activity of the materials also depends upon the electronic structure of the catalysts. Considering the requirement of electron conductivity during the reaction, the presence of electronic band gaps at the Fermi regions would reduce the efficiency of electrocatalyts. Among the 31 2D materials, the electronic structures calculated with GGA-PBE level show metallic behavior for 22 monolayers, as reported in the sixth column of Table 1, whereas the other show electronic band gaps varying from 0.1 in TiS_2 to 1.9 eV in Sb. Since the electronic band gap is known to be generally underestimated by GGA-DFT functionals, we verified the metallic nature for these 22 monolayers by introducing the Hubbard correction term (U).[27–29] Element-specific non-empirical U parameters, as obtained for similar compounds using the self-consistent ACBN0 functional,[29] are adopted for these calculations. An indirect band-gap of around 0.18 eV is observed only for $TiSe_2$. The rest of the monolayers remain metallic in nature (step 3, Figure 1). Figures S3, S4, and S5 in the SI show the electronic band structures for these compounds, calculated with DFT+U functional.

As the last step in the screening process, the stability of the materials in electrochemical environments is determined by computing the aqueous decomposition free energies $\Delta G_{pbx}(\Phi, pH)$ to most stable ionic, molecular, elemental, and solid phases at the applied pH and potential. On the basis of benchmark calculations performed on the compounds analyzed by Singh et. al.,[35] we determined the stability threshold for $\Delta G_{pbx}(\Phi, pH)$ to be up to 0.3 eV/atom within the DFT functional used in this study. The corresponding de-

Table 1: 2D Materials identified as potential catalysts for the HER, as obtained from the first three steps of the computational screening workflow reported in Figure 1. Corresponding overpotential vs RHE for H^+ electrosorption (Φ^{over} in V), aqueous stability ($\Delta G_{pbx}(\Phi, pH)$ in eV/atom), decomposition products (Decomp. pdts), band gap values (E_{gap} in eV) and exfoliation (interlayer binding) energy values in aqueous medium (E_b^{aq} in meV/Å^2) are reported. The pH value is 1, except for those indicated within parentheses in column 3. The exfoliation energies in vacuum (E_b^{vac}) are given in column 7, within parentheses.

Prototype	Compound	Φ^{over}	$\Delta G_{pbx}(\Phi, pH)$	Decomp. pdts	E_{gap}	E_b^{aq} (E_b^{vac})
unary compounds						
Graphite	C	0.3	1.31	CH_4(g)	0.0	17.2 (20.3)
As	P	0.1(4)	3.36	H_3PO_4(aq)	1.9	20.8 (38.2)
	Bi	0.2	0.17	Bi(bulk)	0.6	- (20.1)
	Sb	0.1	0.15	Sb(bulk)	1.2	- (31.5)
binary compounds						
MoS_2 (2-H)	NbS_2	0.1	0.07	$Nb(OH)_5$(aq) + H_2S(aq)	0.0	19.0 (24.2)
	$NbSe_2$	0.2	0.0	$Nb(OH)_5$(aq) + Se(s)	0.0	17.6 (23.4)
	TaS_2	0.2	0.33	Ta_2O_5(aq) + H_2S(aq)	0.0	17.8 (23.1)
	$TaSe_2$	0.5	0.02	Ta_2O_5(aq) + H_2Se(aq)	0.0	16.6 (22.5)
CdI_2 (1-T)	CoO_2	0.1	0.43	Co(s)	0.0	13.2 (22.5)
	MoS_2	0.1(4)	0.1	MoO_2(s) + H_2S(aq)	0.0	23.2 (28.1)
	NbS_2	0.1	0.17	$Nb(OH)_5$(aq) + H_2S(aq)	0.0	17.8 (23.3)
	$NbSe_2$	0.2	0.0	$Nb(OH)_5$(aq) + Se(s)	0.0	17.6 (27.4)
	$NbTe_2$	0.3	0.64	Nb_2O_5(s) + Te(s)	0.0	20.0 (28.4)
	$SiTe_2$	0.4	1.07	SiO_2(s) + Te(s)	0.0	12.4 (19.8)
	$SnSe_2$	0.2	1.6	Sn^{2+}(s) + Se(s)	0.8	8.8 (17.2)
	TaS_2	0.3	0.3	Ta_2O_5(s) + H_2S(aq)	0.0	17.4 (22.4)
	TiS_2	0.4	0.59	TiO_2(s) + H_2S(aq)	0.1	18.8 (23.6)
	$TiSe_2$	0.5	0.27	Ti^{2+}(aq) + H_2Se(aq)	0.0	18.4 (23.9)
	$TiTe_2$	0.2	0.92	TiO_2(s) + Te(s)	0.0	20.2 (28.2)
	VS_2	0.1	0.54	VO^{2+}(aq) + H_2S(aq)	0.0	21.8 (27.9)
	VSe_2	0.2	0.38	VO^{2+}(aq) + Se(s)	0.0	19.0 (25.5)
	VTe_2	0.2	0.54	V_2O_3(s) + Te(s)	0.0	18.2 (26.4)
	$ZrTe_2$	0.3	1.02	ZrO_2(s) + Te(s)	0.0	18.4 (25.8)
FeSe	FeS	0.1	0.0	Fe^{+2}(aq) + H_2S(aq)	0.0	19.6 (25.2)
Bi_2Te_3	Sb_2Te_3	0.5	0.06	$Sb_{16}Te_3$(s) + Te(s)	0.7	14.4 (25.2)
WTe_2	$MoTe_2$	0.3	0.02	Mo_3Te_4(s) + Te(s)	0.0	11.4 (23.05)
	WTe_2	0.5	0.04	WTe_2(bulk)	0.0	13.0 (21.7)
GeS	GeS	0.1(3)	0.17	$HGeO_3^-$(aq) + H_2S(aq)	1.6	24.6 (36.2)
	GeSe	0.1(5)	0.6	$HGeO_3^-$(aq) + HSe^-(aq)	1.1	21.9 (31.9)
Cu_2Te	Cu_2Te	0.1	0.07	CuTe(s) + Te(s)	0.2	- (16.1)
trinary compounds						
Bi_2Te_2S	Zr_2PTe_2	0.1	2.07	ZrO_2(s) + PH_3(g) + Te(s)	0.0	19.2 (26.5)

composition products are given in the fifth column of Table 1. At a pH equal to 1 and at an applied potential equal to the computed electrosorption overpotential, the aqueous decomposition free energies for most of these metallic monolayers are found to exceed the stability threshold value (fourth column of Table 1). However, by exploiting the grand potential approach we can systematically vary the electrochemical environment in order to identify conditions for which both the catalytic activity is high and the material is stable with respect to electrochemical decomposition. Thus, we calculated the $\Delta G_{pbx}(\Phi, pH)$ and H^+ electrosorption possibilities for pH values ranging from 1 to 7 and overpotentials from 0 V up to 0.5 V vs. RHE. Out of the 21 compounds considered in this last screening step, 15 materials are found to present one region of stability within the aforementioned ranges of environment conditions (step 4, Figure 1). Figure 3 shows the stability plots for these monolayers, which could be stabilized by tuning the pH of the medium within the catalytically active region denoted as the unshaded area. In this region, the H^+ electrosorption free energies vary between -0.1 to 0.1 eV/H. For the other 6 monolayers i.e., $NbTe_2$, $SiTe_2$, $TiTe_2$, $ZrTe_2$, Graphene(C) and Zr_2PTe_2, the stability region ($\Delta G_{pbx}(\Phi, pH) < 0.3$ eV/atom) does not coincide with the catalytically active region up to an overpotential of 0.5 V vs. RHE. The corresponding plots for these are shown in supporting Figure S6. The atomistic details of hydrogen absorption on the two best performing materials (CoO_2 and FeS) are reported in Figure 4, together with a visualization of the interfaces of the continuum embeddings.

It is important to notice that all of the identified materials have vacuum exfoliation energies in a relatively narrow range of $E_b^{vac} = 25 \pm 5$ meV/^{2} (green overcircles in Figure 2). As this quantity can be easily accessed by simulations in vacuum, it can represent an important screening criteria in future studies of layered materials. However, from the results in Figure 2 it is also evident that this descriptor cannot be used alone to characterize the full performance of a material: several materials that have exfoliation energies in the ideal range fail to pass the screening process when the effects of electrochemical environments are explicitly accounted for.

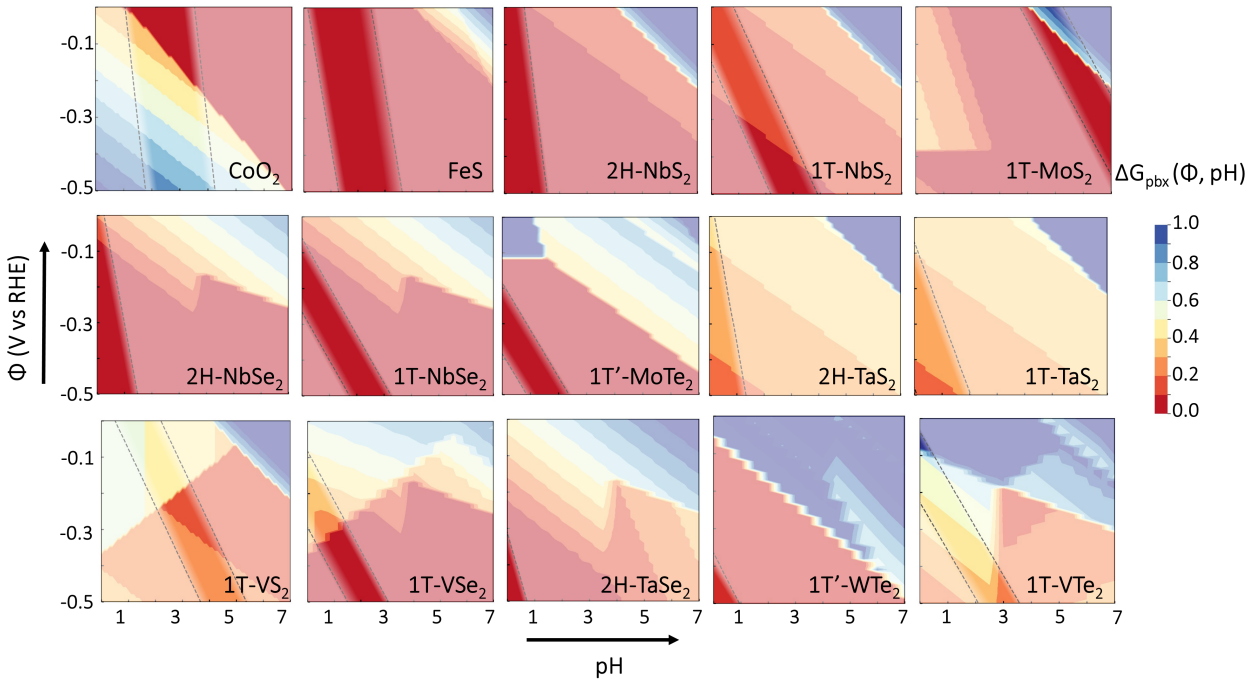

Figure 3: Plots of stability vs. environment conditions (applied potential Φ vs. RHE and pH) for the 15 compounds that passed all of the screening steps. The catalytically active region, for which reversible H^+ electrosorption free energies between -0.1 to 0.1 eV/H are obtained, is shown as the unshaded area. The colormap of the plots refers to the aqueous decomposition free energies $\Delta G_{pbx}(\Phi, pH)$ with respect to the most stable compound-specific ionic, molecular, elemental, and solid decomposition products.

Within the identified compounds, $\Delta G_{pbx}(\Phi, pH)$ shows large variations within the catalytically active region, which allows the identification of three subclasses of materials. The eight monolayers CoO_2, FeS, 2H-NbS_2, 1T-NbS_2, 2H-$NbSe_2$, 1T-$NbSe_2$ 1T-MoS_2, and 1T′-$MoTe_2$, show the maximum efficiency and greater stability within the catalytically active region. The overpotential values could be lowered near to zero by tuning the pH of the medium. On the other hand, 2H-TaS_2, 1T-TaS_2, 1T-VS_2, and 1T-VSe_2 show slightly lower aqueous stability at lower overpotential values. For these compounds, the catalytic efficiency could be improved by reducing the surface reactivity to different aqueous ions. One possibility would be using non-aqueous solvents with slightly less polarity compared to water. The remaining three monolayers, 2H-$TaSe_2$, 1T′-WTe_2, and 1T-VTe_2, show the lowest efficiency. The best catalytic activity for these compounds is obtained within a very narrow range of potentials, at low pH values.

The screening workflow reported here only relies on simulations performed in vacuum or in continuum environments. Even though the continuum approximation might underestimate the role of specific solute-solvent interactions, it was recently shown that hybrid continuum-based approaches featuring one layer of explicit solvent molecules are able to provide accurate results for complex electronic properties of the substrates, such as the alignment of band edges of semiconductors.[36,37] While hybrid simulations do not easily lend themselves to a systematic screening of materials, they can be used to check for significant deviations from purely continuum approaches. Hybrid calculations on simplified realizations of water interfaces for the two best performing materials (CoO_2 and FeS) are performed and the detailed results are reported in SI Section S-VII. For FeS, hydrogen adsorption does not appear to be substantially affected by the inclusion of explicit water molecules. However, specific hydrogen-bond interactions play a more evident role in stabilizing hydrogen adsorption on the CoO_2 surface. This is due to a better match between a hydrogen-bonded overlaying water network and the substrate lattice. This stabilization would shift the catalytic active region of Figure 3 towards higher pH with respect to the values computed from

purely continuum simulations. While an accurate characterization of the magnitude of the shift would require more extensive molecular dynamics simulations,[38,39] the average stabilization obtained on the considered models would correspond to a shift of the catalytic active region around neutral pH values. As the material stability is predicted to increase at higher pH, we expect this stabilization to not affect the overall ranking of the identified catalysts.

In order to suggest effective synthetic pathways, we computed the exfoliation (interlayer binding) energies in aqueous medium for the van der Waals solids from which these monolayers could be exfoliated, as reported in column 7 of Table 1. The values denoted within parentheses are obtained without the inclusion of solvent effects, which are in good agreement with the values reported earlier by Mounet et. al.[4] The exfoliation energy values in aqueous medium are calculated using the following equation

$$E_b^{aq} = \frac{1}{A} J(\Phi), \tag{2}$$

where A is the interfacial area. While the accuracy of these results can significantly depend on the values of the empirical parameters that enter in the definition of the continuum embedding, benchmark simulations for the binding energy of graphene computed with the parameters proposed by Hörmann et al. for electrochemical interfaces[23] show good agreement with recently reported experimental solvation free energy.[40] Further details on the calculations are reported in the SI.

Values of E_b^{aq} for the three materials Bi, Sb, and Cu_2Te are not obtained. The two unary 2D materials (Bi and Sb) could not be exfoliated from the reference 3D-solid taken for the grand-potential energy calculation, since the corresponding 3D-structures do not have van der Waals layered arrangement. On the other hand, 2D-Cu_2Te undergoes significant surface reconstruction compared to its bulk van der Waals structure. Therefore, the interfacial energy obtained for this compound would be slightly different from the exfoliation energy value. The electrostatic interaction with the solvent reduces the interlayer binding energies

for the other 3D-bulk solids to great extent. Among the identified 15 metallic monolayers with better HER catalyzing efficiency, the three compounds 1T′-$MoTe_2$, 1T′-WTe_2 and CoO_2 show the lowest E_b^{aq} of 11.4, 13.0 and 13.2 meV/Å^2 respectively. The highest E_b^{aq} of around 21.8 meV/Å^2 is obtained for 1T-VS_2. In average, the aqueous exfoliation energies are almost similar to that obtained for graphene in the presence of an aqueous solvent. Lowering of interlayer binding strength would enable the separation of the layers with liquid phase exfoliation methods, using for instance the sonication technique or electrochemical methods after ion intercalation. Moreover, alternative synthetic pathways, such as the chemical vapor deposition method on selected substrates could be possible since these monolayers show considerably high dynamic stabilities.

In summary, we reported the HER electrocatalytic efficiency and the aqueous stability of recently proposed 258 easily exfoliable monolayers. By screening these materials for the H^+ adsorption possibilities at different surface sites, 64 2D materials are identified as suitable for H^+ electrosorption reaction in vacuum. The inclusion of solvent polarization and the effect of electrolyte charges reduces the adsorption free energies to large extent. We found that 31 materials are suitable, which shows the requirement of relatively lower overpotentials at acidic pH. Considering the metallic nature and the aqueous stability in presence of different aqueous ions, 15 monolayers are selected, whose catalytic efficiency can be effectively tuned by varying the pH of the medium. While most of these 2D materials show interesting efficiencies, CoO_2 and FeS can be proposed as the most promising alternatives to Pt-electrodes. Both these monolayers are composed of earth abundant elements and show a wide stability range at reducing potentials. Moreover, by tuning the pH of the medium, the overpotential for the H^+ ions can be reduced to be near to zero. Based upon the aqueous exfoliation energies with respect to the corresponding 3D van der Waals solids, possible synthesizing strategies are suggested for these 2D materials.

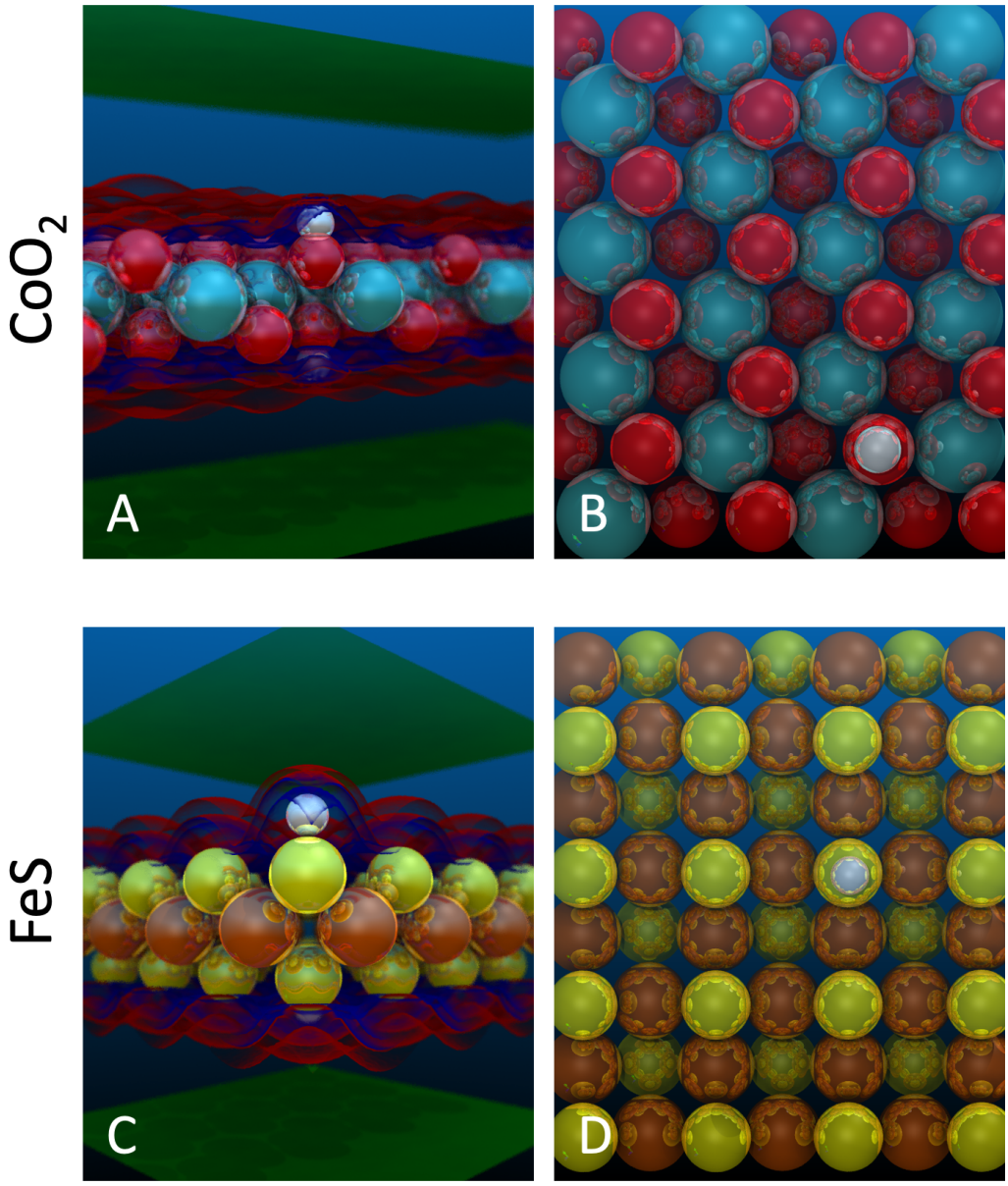

Figure 4: Side (A and C) and top (B and D) views of the CoO_2 and FeS surfaces with a H^+ ion adsorbed on the most preferred sites (atop of O and S atoms, respectively). The details of the continuum embedding environment are also visualized in panels A and C as colored transparent isosurfaces. In particular, the polarization charges associated with the continuum dielectric embedding are shown by red/blue isosurfaces, whereas the charge of the electrochemical diffuse layer, as described by a numerical Gouy-Chapman-Stern model, is shown in green.

Supporting Information Available

The Supporting Information (SI) is available free of charge on the ACS Publications website at DOI: XXXX

The computational grand potential simulation methodologies for calculating the H^+ electrosorption free energies on the 2D-material surfaces with continuum embedding and the aqueous binding energies, E_b^{aq} of 2D materials from the corresponding 3D van-der-Waals solids have been described in section S-I, S-II, and S-III. The aqueous stability with respect to different aqueous species is provided in the section S-IV. The bandstructures of the 15 best performing materials are shown in Figure S4 and S5, section S-V. The Figure S6, section S-VI shows the stability plots for the six 2D materials found to be unstable in the catalytically active region. The hybrid-continuum simulations methodologies for CoO_2 and FeS are given in section S-VII.

Acknowledgement

We acknowledge computational support and resources from the computing facilities at University of North Texas (UNT), the Center for Advanced Scientific Computing and Modeling (CASCaM), the National Energy Research Scientific Computing Center (NERSC) at Lawrence Berkeley National Laboratory, and the Center for Nanophase Materials Sciences (CNMS) at Oak Ridge National Laboratory .

References

(1) Turner, J. A. Sustainable Hydrogen Production. *Science* **2004**, *305*, 972 LP – 974.

(2) Vesborg, P. C. K.; Seger, B.; Chorkendorff, I. Recent Development in Hydrogen Evolution Reaction Catalysts and Their Practical Implementation. *J. Phys. Chem. Lett.* **2015**, *6*, 951–957.

(3) Seh, Z. W.; Kibsgaard, J.; Dickens, C. F.; Chorkendorff, I.; Nørskov, J. K.; Jaramillo, T. F. Combining theory and experiment in electrocatalysis: Insights into materials design. *Science* **2017**, *355*.

(4) Mounet, N.; Gibertini, M.; Schwaller, P.; Campi, D.; Merkys, A.; Marrazzo, A.; Sohier, T.; Castelli, I. E.; Cepellotti, A.; Pizzi, G.; Marzari, N. Two-dimensional materials from high-throughput computational exfoliation of experimentally known compounds. *Nat. Nanotech.* **2018**, *13*, 246–252.

(5) Chia, X.; Eng, A. Y. S.; Ambrosi, A.; Tan, S. M.; Pumera, M. Electrochemistry of nanostructured layered transition-metal dichalcogenides. *Chem. rev.* **2015**, *115*, 11941–11966.

(6) Chia, X.; Pumera, M. Layered transition metal dichalcogenide electrochemistry: journey across the periodic table. *Chem. Soc. Rev.* **2018**, *47*, 5602–5613.

(7) Li, P.; Zhu, J.; Handoko, A. D.; Zhang, R.; Wang, H.; Legut, D.; Wen, X.; Fu, Z.; Seh, Z. W.; Zhang, Q. High-throughput theoretical optimization of the hydrogen evolution reaction on MXenes by transition metal modification. *J. Mater. Chem. A* **2018**, *6*, 4271–4278.

(8) Yang, J.; Shin, H. S. Recent advances in layered transition metal dichalcogenides for hydrogen evolution reaction. *J. Mater. Chem. A* **2014**, *2*, 5979–5985.

(9) Cheon, G.; Duerloo, K.-A. N.; Sendek, A. D.; Porter, C.; Chen, Y.; Reed, E. J. Data mining for new two-and one-dimensional weakly bonded solids and lattice-commensurate heterostructures. *Nano Lett.* **2017**, *17*, 1915–1923.

(10) Choudhary, K.; Kalish, I.; Beams, R.; Tavazza, F. High-throughput Identification and Characterization of Two-dimensional Materials using Density functional theory. *Sci. Rep.* **2017**, *7*, 5179.

(11) Ashton, M.; Paul, J.; Sinnott, S. B.; Hennig, R. G. Topology-Scaling Identification of Layered Solids and Stable Exfoliated 2D Materials. *Phys. Rev. Lett.* **2017**, *118*, 106101.

(12) Haastrup, S.; Strange, M.; Pandey, M.; Deilmann, T.; Schmidt, P. S.; Hinsche, N. F.; Gjerding, M. N.; Torelli, D.; Larsen, P. M.; Riis-Jensen, A. C.; Gath, J.; Jacobsen, K. W.; Mortensen, J. J.; Olsen, T.; Thygesen, K. S. The Computational 2D Materials Database: high-throughput modeling and discovery of atomically thin crystals. *2D Mater.* **2018**, *5*, 42002.

(13) Zhou, J.; Shen, L.; Costa, M. D.; Persson, K. A.; Ong, S. P.; Huck, P.; Lu, Y.; Ma, X.; Chen, Y.; Tang, H.; Feng, Y. P. 2DMatPedia, an open computational database of two-dimensional materials from top-down and bottom-up approaches. *Sci. Data* **2019**, *6*, 86.

(14) Liu, H.; Sun, J.-T.; Liu, M.; Meng, S. Screening magnetic two-dimensional atomic crystals with nontrivial electronic topology. *J. Phys. Chem. Lett.* **2018**, *9*, 6709–6715.

(15) Rasmussen, F. A.; Thygesen, K. S. Computational 2D materials database: electronic structure of transition-metal dichalcogenides and oxides. *J. Phys. Chem. C* **2015**, *119*, 13169–13183.

(16) Ataca, C.; Sahin, H.; Ciraci, S. Stable, single-layer MX2 transition-metal oxides and dichalcogenides in a honeycomb-like structure. *J. Phys. Chem. C* **2012**, *116*, 8983–8999.

(17) Jain, A.; Wang, Z.; Norskov, J. K. Stable Two-dimensional Materials for Oxygen Reduction and Oxygen Evolution Reactions. *ACS Energy Lett.* **2019**, *4*, 1410–1411.

(18) Magnussen, O. M.; Groß, A. Toward an atomic-scale understanding of electrochemical interface structure and dynamics. *J. Am. Chem. Soc.* **2019**, *141*, 4777–4790.

(19) Frediani, L.; Andreussi, O.; Kulik, H. J. Coding solvation: challenges and opportunities. *Int. J. Quantum Chem.* **2019**, *119*, e25839.

(20) Andreussi, O.; Dabo, I.; Marzari, N. Revised self-consistent continuum solvation in electronic-structure calculations. *J. Chem. Phys.* **2012**, *136*, 064102.

(21) Fisicaro, G.; Genovese, L.; Andreussi, O.; Marzari, N.; Goedecker, S. A generalized Poisson and Poisson-Boltzmann solver for electrostatic environments. *J. Chem. Phys.* **2016**, *144*, 014103.

(22) Nattino, F.; Truscott, M.; Marzari, N.; Andreussi, O. Continuum models of the electrochemical diffuse layer in electronic-structure calculations. *J. Chem. Phys.* **2019**, *150*, 041722.

(23) Hörmann, N. G.; Andreussi, O.; Marzari, N. Grand canonical simulations of electrochemical interfaces in implicit solvation models. *J. Chem. Phys.* **2019**, *150*, 041730.

(24) Kohn, W.; Sham, L. J. Self-Consistent Equations Including Exchange and Correlation Effects. *Phys. Rev.* **1965**, *140*, A1133–A1138.

(25) Gouy, M. Sur la constitution de la charge électrique à la surface d'un électrolyte. *J. Phys. Theor. Appl.* **1910**, *9*, 457–468.

(26) Chapman, D. L. LI. A contribution to the theory of electrocapillarity. *Philos. Mag.* **1913**, *25*, 475–481.

(27) Anisimov, V. I.; Aryasetiawan, F.; Lichtenstein, A. First-principles calculations of the electronic structure and spectra of strongly correlated systems: the LDA+ U method. *J. Phys.: Condens. Matter* **1997**, *9*, 767.

(28) Liechtenstein, A. I.; Anisimov, V. I.; Zaanen, J. Density-functional theory and strong interactions: Orbital ordering in Mott-Hubbard insulators. *Phys. Rev. B* **1995**, *52*, R5467–R5470.

(29) Agapito, L. A.; Curtarolo, S.; Buongiorno Nardelli, M. Reformulation of DFT + U as a

Pseudohybrid Hubbard Density Functional for Accelerated Materials Discovery. *Phys. Rev. X* **2015**, *5*, 011006.

(30) Parsons, R. The rate of electrolytic hydrogen evolution and the heat of adsorption of hydrogen. *Trans. Faraday Soc.* **1958**, *54*, 1053–1063.

(31) Li, H.; Tsai, C.; Koh, A. L.; Cai, L.; Contryman, A. W.; Fragapane, A. H.; Zhao, J.; Han, H. S.; Manoharan, H. C.; Abild-Pedersen, F.; Nørskov, J. K.; Zheng, X. Activating and optimizing MoS2 basal planes for hydrogen evolution through the formation of strained sulphur vacancies. *Nat. Mater.* **2015**, *15*, 48.

(32) Voiry, D.; Yamaguchi, H.; Li, J.; Silva, R.; Alves, D. C. B.; Fujita, T.; Chen, M.; Asefa, T.; Shenoy, V. B.; Eda, G.; Chhowalla, M. Enhanced catalytic activity in strained chemically exfoliated WS2 nanosheets for hydrogen evolution. *Nat. Mater.* **2013**, *12*, 850.

(33) Greeley, J.; Jaramillo, T. F.; Bonde, J.; Chorkendorff, I.; Nørskov, J. K. Computational high-throughput screening of electrocatalytic materials for hydrogen evolution. *Nat. Mater.* **2006**, *5*, 909–913.

(34) Chia, X.; Ambrosi, A.; Lazar, P.; Sofer, Z.; Pumera, M. Electrocatalysis of layered Group 5 metallic transition metal dichalcogenides (MX 2, M= V, Nb, and Ta; X= S, Se, and Te). *J. Mater. Chem. A* **2016**, *4*, 14241–14253.

(35) Singh, A. K.; Zhou, L.; Shinde, A.; Suram, S. K.; Montoya, J. H.; Winston, D.; Gregoire, J. M.; Persson, K. A. Electrochemical stability of metastable materials. *Chem. Mater.* **2017**, *29*, 10159–10167.

(36) Hörmann, N. G.; Guo, Z.; Ambrosio, F.; Andreussi, O.; Pasquarello, A.; Marzari, N. Absolute band alignment at semiconductor-water interfaces using explicit and implicit descriptions for liquid water. *npj Comput Mater* **2019**, *5*, 1–6.

(37) Blumenthal, L.; Kahk, J. M.; Sundararaman, R.; Tangney, P.; Lischner, J. Energy level alignment at semiconductor–water interfaces from atomistic and continuum solvation models. *RSC adv.* **2017**, *7*, 43660–43670.

(38) Ambrosio, F.; Wiktor, J.; Pasquarello, A. pH-Dependent Surface Chemistry from First Principles: Application to the BiVO4 (010)–Water Interface. *ACS Appl. Mater. interfaces* **2018**, *10*, 10011–10021.

(39) Cheng, J.; Sprik, M. Alignment of electronic energy levels at electrochemical interfaces. *Phys. Chem. Chem. Phys.* **2012**, *14*, 11245–11267.

(40) van Engers, C. D.; Cousens, N. E.; Babenko, V.; Britton, J.; Zappone, B.; Grobert, N.; Perkin, S. Direct measurement of the surface energy of graphene. *Nano Lett.* **2017**, *17*, 3815–3821.